Analysis of Stator End-winding in a Dual Wound Machine Using Biot-Savart Law

Boyuan Yin[1], Xiaoze Pei[1*], John Frederick Eastham[1], Xianwu Zeng[2]

[1]Department of Electronic & Electrical Engineering, University of Bath, Bath, United Kingdom
[2]Department of Mechanical Engineering, University of Bath, Bath, United Kingdom
**X.Pei@bath.ac.uk*

Keywords: DUAL WOUND MACHINE, END-WINDING, BIOT-SAVART LAW

Abstract

Integrated full electric propulsion (IFEP) systems provide both ship propulsion and services with different electrical ratings. Instead of using multiple electrical machine sets, a dual wound machine with two sets of windings sharing the same stator slots can use one prime mover to provide two independent power supplies, achieving a more compact design and maximizing the power density. In order to provide independent power supplies, the windings must eliminate the electromagnetic coupling between them. A 2-pole and 6-pole dual wound machine has been designed previously. The simulation results show that there is no electromagnetic coupling considering the windings in the slots. It is important to investigate if there is any electromagnetic coupling caused by the end-windings. This paper proposes a simplified 2D and 3D end-winding model to analyse the magnetic field distribution and induced voltage using the Biot-Savart law. It is concluded that the end-windings of the dual wound machine are also not electromagnetically coupled, which proves that it is able to produce two independent power supplies for ship propulsion and services.

1 Introduction

Integrated full electric propulsion (IFEP) system has great benefits on large cruise ships and naval warships. It can achieve more impact arrangement, reduce fuel consumption, enhance dynamic performance and increase the system reliability [1] – [4]. Compared with the general IFEP system with multiple electrical machine sets, a dual wound machine can produce two outputs with different power ratings and only require one prime mover, which can save space on the ships. A 2-pole and 6-pole dual wound machine for electric ships has been designed previously [5]. The in-slot windings have been analysed to show that the two outputs are decoupled. However, the end-winding analysis has to be considered because they could have mutual coupling. The end-windings also generate excessive electromagnetic force causing vibration and have a negative influence on the insulations. Therefore, it is worthwhile to investigate the influence of the end-windings on the dual wound machine.

Some studies on electric machine end-windings have been proposed [6] – [7]. Research work on end-winding forces influenced by rotor currents was performed in 1988 [8], in which the Biot-Savart law was applied, and the comparison of calculated results and experimental measurements demonstrated a good agreement. There are also studies based on the 3D finite element method (FEM) that can provide more precise magnetic field distributions especially close to the ferromagnetic materials [6]. However, a 3D FEM with end-winding is very complicated and takes a long time to solve.

This paper proposes a simplified and efficient 2D model to calculate the induced voltage between the end-windings and enable the investigation of winding inductance. A 3D model is also proposed to further analyse the magnetic field distribution. allowing the radial-direction distance between the rotor and stator windings to be considered. The calculations in this paper are based on the Biot-Savart law.

2. ANALYTICAL MODEL

2.1 Biot-Savart Law and Mathematical Equations

To obtain the magnetic flux density on a certain point produced by a current element idl, the Biot-Savart law can be expressed as

$$dB = \frac{\mu_0}{4\pi} i \frac{dl \times \vec{r}}{r^3} \tag{1}$$

Where $\vec{r}$ is the position vector from the current element pointing to the calculation point. μ_0 is the vacuum permeability.

The integration of equation 1 can be simplified and expressed as equation 2, which can be used to calculate the magnetic flux density on a certain point.

$$\vec{B} = \frac{\mu_0}{4\pi} I \int_L \frac{sin\theta \cdot dl}{r^2} \vec{e} \tag{2}$$

Where θ is the angle between the current element idl and the position vector $\vec{r}$. $\vec{e}$ is the unit vector.

In a very small region, the magnetic flux density can be regarded being constant, therefore the magnetic flux can be calculated by

$$d\emptyset = B \cdot dA \tag{3}$$

Where $\emptyset$ is the magnetic flux and A is the calculation area.

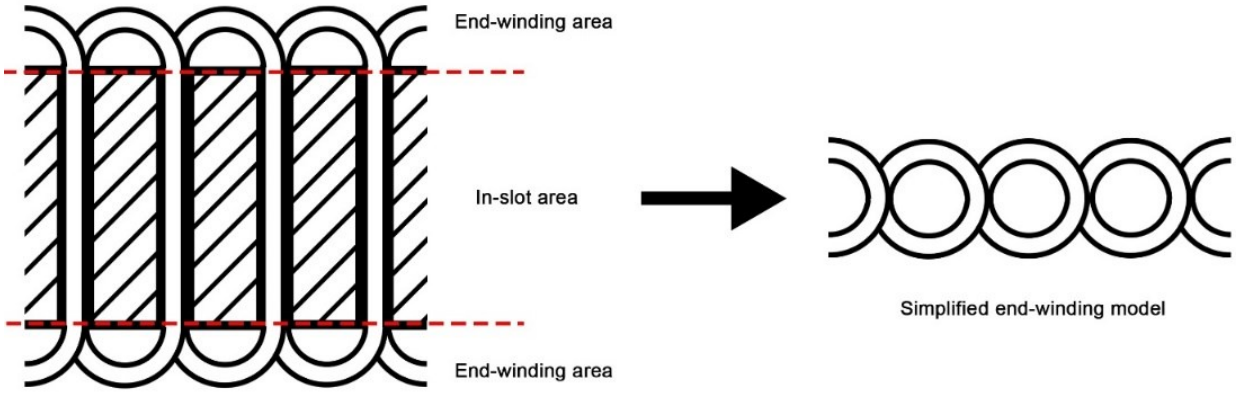

Fig. 1 Simplified 2D end-winding model

According to Faraday's law, the induced voltage of any end-winding coil can be calculated as

$$\varepsilon = -N\frac{d\emptyset}{dt} \tag{4}$$

Where ε is the coil induced voltage. N is the number of turns.

Then the coil inductance can be calculated for an inductor:

$$v = L\frac{di}{dt} \tag{5}$$

2.2 End-windings Topology and Modelling Method in 2D

The end-winding topology of electric machine is normally complex and difficult to analyse. An analytical method is proposed to use a simplified model to evaluate the effect of the end-windings. The iron core and the in-slot coils are ignored a simplification which is commonly used in electric machine analysis. Fig. 1 shows the simplified end-windings topology, which are circle-shaped coils considering both sides of the end-windings. To apply the Biot-Savart law, each coil of the end-windings is replaced by an equivalent filamentary conductor using the original number of turns.

Fig. 2 shows the stator winding distribution of the dual wound machine designed in the previous paper [5]. The machine uses double layer windings with a pitch of 12 slots for the two pole and a pitch of 5 slots for the six. The different colours indicate the coil pitch. The arrangement aims to maximize the induced voltage and eliminate any mutual air gap flux density space harmonics between the windings so that there is no electromagnetic coupling between them. The previous research has shown that the arrangement is successful and that the in-slot windings can work independently without mutual coupling. However, the end-windings still have to be considered.

According to the winding distribution table in Fig. 2, Fig. 3 shows the simplified end-winding model with three phases noted in red, blue and green. This structure is built by simplifying the 3D end-winding model onto a 2D plane. The boundaries on the two ends are connected.

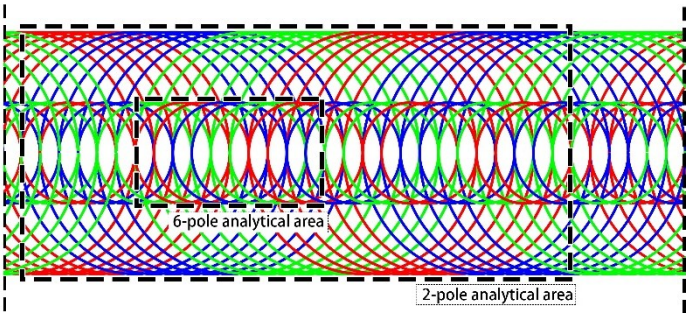

Fig. 3 2-pole and 6-pole end-windings distribution in 2D

2.3 End-windings Topology and Modelling Method in 3D

The simplified 2D model is fast and efficient to implement. However, the model is based on the assumption that the dual windings are on the same plane. To consider the end-winding 3D topology effect and the radial-direction distance between the rotor and stator, a simplified 3D model based on the Biot-Savart law is proposed in this paper. As shown in Fig. 4, the practical end-coil is represented by a filamentary conductor (the blue and red curve) above the airgap conductor (the

Slot	1	2	3	4	5	6	7	8	9	10	11	12	13	14	15	16	17	18	19	20	21	22	23	24	25	26	27	28	29	30	31	32	33	34	35	36
2 Pole	R	R	R	R	R	R	-B	-B	-B	-B	-B	-B	Y	Y	Y	Y	Y	Y	-R	-R	-R	-R	-R	-R	B	B	B	B	B	B	-Y	-Y	-Y	-Y	-Y	-Y
	-B	-B	-B	-B	-B	-B	Y	Y	Y	Y	Y	Y	-R	-R	-R	-R	-R	-R	B	B	B	B	B	B	-Y	-Y	-Y	-Y	-Y	-Y	R	R	R	R	R	R
6 Pole	R	R	-B	-B	Y	Y	-R	-R	B	B	-Y	-Y	R	R	-B	-B	Y	Y	-R	-R	B	B	-Y	-Y	R	R	-B	-B	Y	Y	-R	-R	B	B	-Y	-Y
	R	-B	-B	Y	Y	-R	-R	B	B	-Y	-Y	R	R	-B	-B	Y	Y	-R	-R	B	B	-Y	-Y	R	R	-B	-B	Y	Y	-R	-R	B	B	-Y	-Y	R

Fig. 2 2-pole and 6-pole windings distribution

yellow curve). The magnetic field distribution in the analytical area can be calculated in a similar to 2D model, but the effective coil area becomes more complex as it is a cylindrical surface.

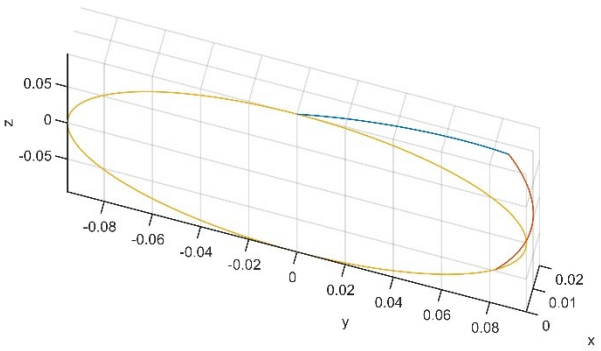

Fig. 4 Filamentary end-winding conductor in 2D

Fig. 5 presents all the end-windings for the 2-pole generator based on the winding distribution in Fig. 2. The main difference between this simplified 3D Biot-Savart law model and the 3D finite element model is that the end-coils are replaced by the filamentary conductors, which is much easier to calculate and saves significant computational time. However, the drawback is obvious; the effect of the magnetic core is not considered. The magnetic field close to the airgap may not be accurate as this model assumes all conductors are in an infinite air space. However, most parts of the end-windings are remote from the magnetic core, thus the magnetic field around the end-winding area is still meaningful.

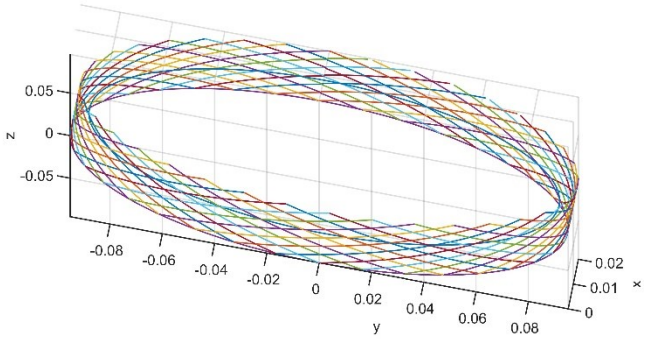

Fig. 5 2-pole end-windings distribution in 3D

3 STATOR END-WINDINGS ANALYSIS

Based on the structure shown in Fig. 3, the magnetic flux density on each position in the effective area can be calculated by the analytical method proposed above. In order to calculate the total magnetic flux through each coil, the analytical area has to be meshed as the first step. And then integrate each mesh element to calculate the total magnetic flux. Fig. 6 shows the magnetic field produced by the 2-pole end-windings. The magnetic field is only calculated in the 2-pole analytical area shown in Fig. 3. The exciting current through each coil is sinusoidal with a peak current of 6A to match the original machine design. Each 2-pole end-winding coil has 8 turns. Using these parameters, the 2-pole back-EMF and the self and mutual inductance can be calculated.

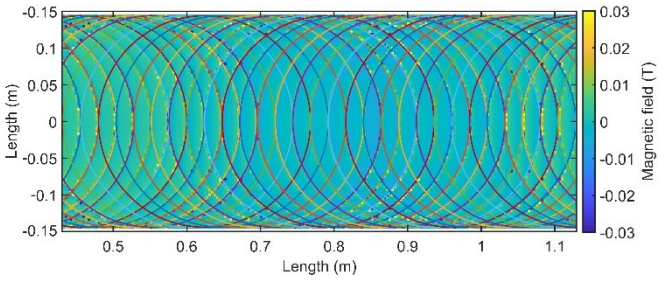

Fig. 6 2-pole magnetic field distribution

Fig. 7 shows the magnetic field produced by the 6-pole end-windings. The magnetic field is only calculated in the 6-pole analytical area shown in Fig. 3. Each 6-pole end-winding coil has 6 number of turns. The exciting current through each coil is sinusoidal with peak current of 4A.

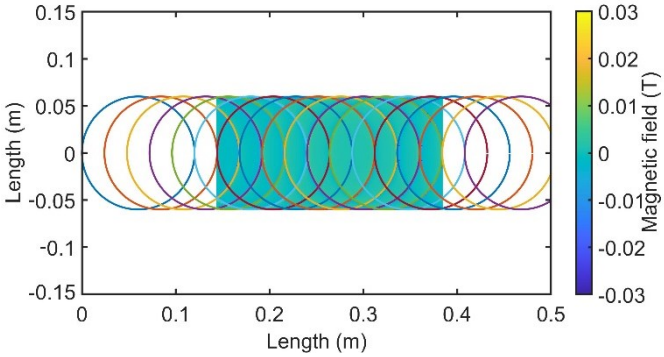

Fig. 7 6-pole magnetic field distribution

The induced voltage of the end-windings at each time step can be calculated from the magnetic field distribution in the analytical area is shown in Fig. 6 and Fig. 7. Fig. 8 shows the induced voltage in the 2-pole and 6-pole end-windings generated by the 2-pole stator magnetic field. The 2-pole stator end-windings has back-emf of around 3 V peak voltage whilst the 6-pole end-winding induced voltage produced by the 2-pole end-windings is almost zero. This indicates that the 2-pole end-winding is decoupled from 6-pole end-winding.

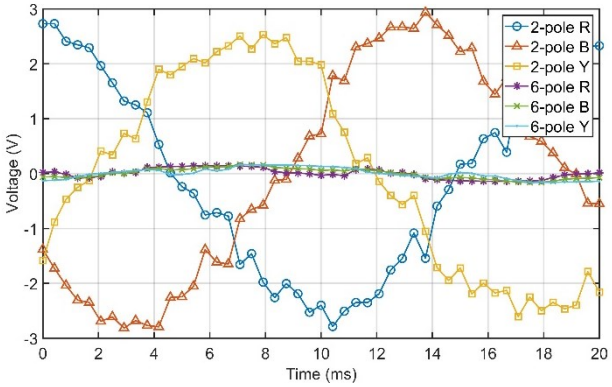

Fig. 8 Induced voltage by 2-pole stator windings

To consider the end-winding 3D topology effect and the radial-direction distance between the rotor and stator, a simplified 2-pole end-windings 3D model is built as shown in Fig. 5. The benefit of the 3D Biot-Savart model is that the magnetic field distributed around the end-windings can be calculated. Fig. 9

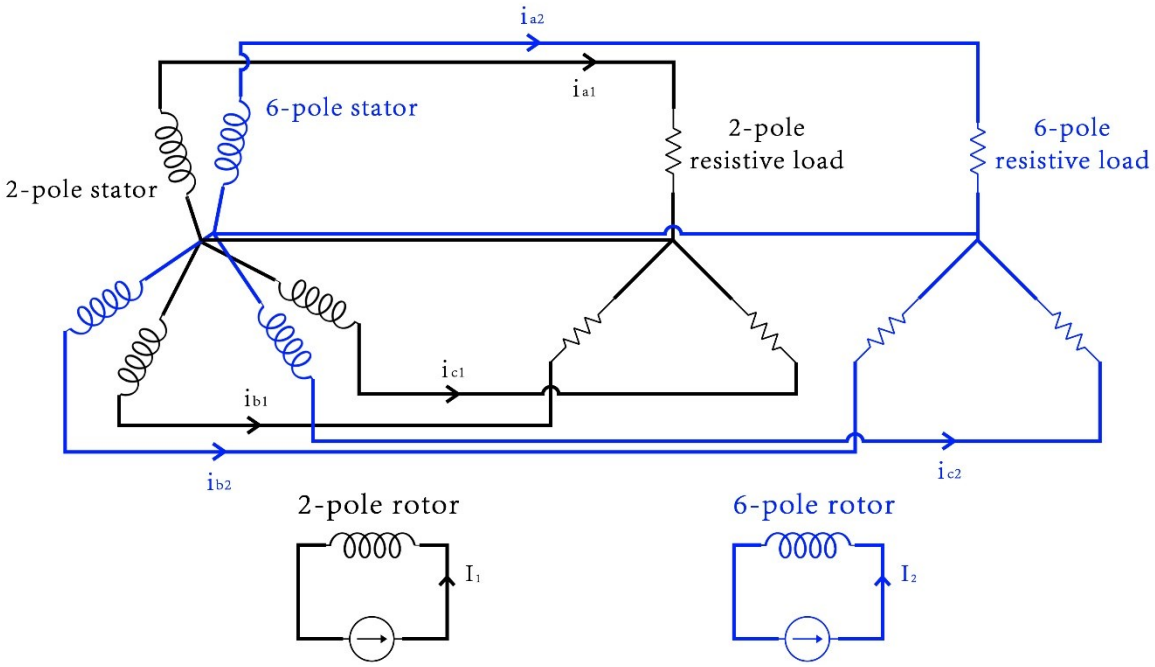

Fig. 11 Electric connection of the dual wound generator

presents the magnetic field distribution along a track near the end-windings, which has the radial distance of 5mm from the end-windings and 10mm from the magnetic core. The magnetic field on each calculation point can be analysed by three components: radial flux density (B_r), tangential flux density (B_θ) and axial flux density (B_Z). The induced voltage can be further investigated using 3D model.

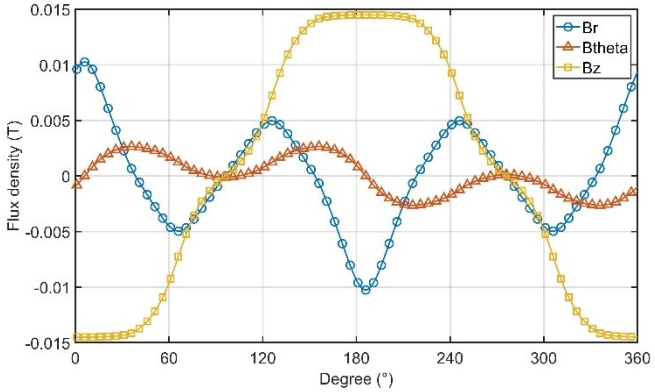

Fig. 9 Magnetic field distribution around 3D end-windings

4 EXPERIMENTAL PLATFORM

A dual wound generator prototype based on the design was built with the dimension shown in Table. I to verify the simulation results. The experimental platform of the designed dual wound machine prototype is shown in Fig. 10. This dual wound generator was rewound using the existing machine frame and the proposed winding design in Fig. 2.

Due to the machine topology, it is not possible to experimentally measure the voltage induced in the end-winding separately. The total voltage including the in-slot winding and the end-windings can be measured to verify the whole winding is decoupled. And the magnetic field near the end-windings can be experimentally measured to match the results with the 2D and 3D Biot-Savart law model.

Table 1 Generator dimensions

Item	Stator	Rotor
Number of slots	36	24
Diameter	190.5 mm	186.5 mm
Axial length	123.6 mm	139.5 mm
Slot opening	2.7 mm	3.5 mm
Airgap	2 mm	
Stator outer diameter	295 mm	

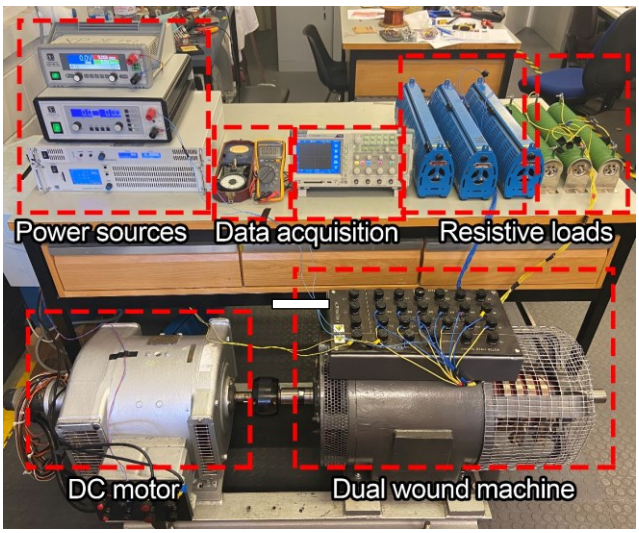

Fig. 10 Experimental platform

The 2-pole and 6-pole stator windings are connected with 3-phase resistive loads separately as shown in Fig. 11. The two rotor windings are excited by 1A DC current supply.

Fig. 12 shows the 2-pole and 6-pole stator terminal voltages when only the 2-pole rotor is excited. This result takes into

account both the in-slot windings and the end-windings. The 2-pole stator has peak voltage of around 170 V and the voltage on 6-pole winding is negligible.

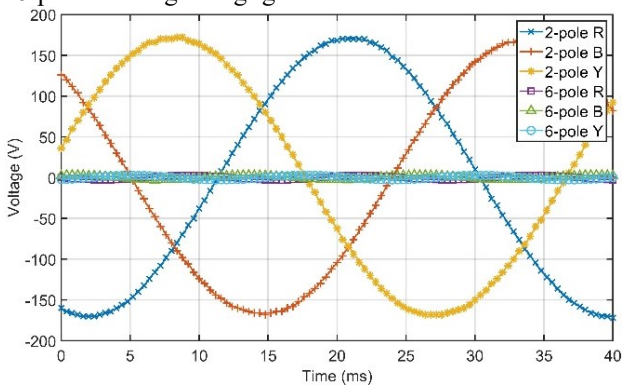

Fig. 12. 2-pole and 6-pole stator voltage with 2-pole excitation

Fig. 13 shows the 2-pole and 6-pole stator terminal voltage when only 6-pole rotor is excited. The 6-pole stator has peak voltage of around 132 V and the voltage on 2-pole winding is negligible.

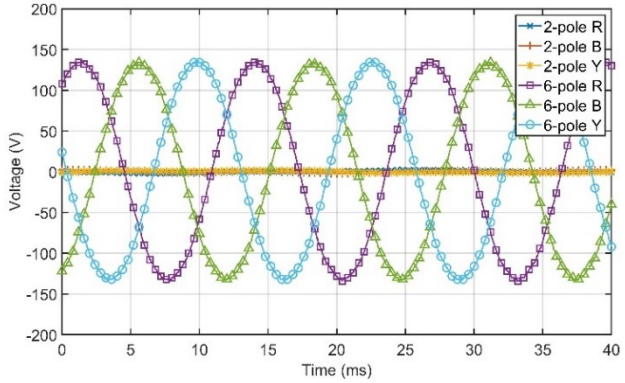

Fig. 13. 2-pole and 6-pole stator voltage with 6-pole excitation

When both 2-pole and 6-pole rotor windings are excited as shown in Fig. 14, both windings can generate voltage independently. This experimental result shows that the three-phase outputs are balanced without the influence of the other winding.

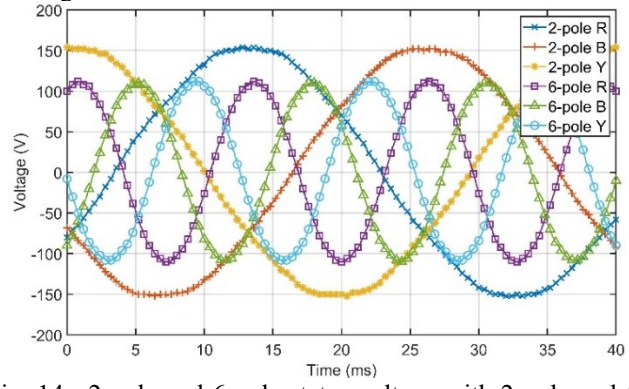

Fig. 14. 2-pole and 6-pole stator voltage with 2-pole and 6-pole excitation

5 CONCLUSIONS AND FUTURE WORK

This paper focuses on the design methodology to analyse the stator end-winding effects in a dual wound machine topology. The analytical method is proposed to simplify the calculation using a 2D model with filamentary conductors. Also, a 3D model is proposed to consider the end-winding 3D topology effect and the radial-direction distance between the rotor and stator. Biot-Savart law is used to analyse the magnetic field distribution and induced voltage for the end-windings. A prototype dual wound generator based on the design has been rewound and experimentally tested to verify the analysis and design. The dual wound generator prototype demonstrates that the 2-pole and 6-pole end-windings can generate individual power outputs without influence from the other winding. Both the analytical modelling and the experimental results show the 2-pole and 6-pole end-windings are decoupled.

6 References

[1] J. M. Apsley, A. Gonzalez-Vill asenor, M. Barnes, A. C. Smith, S. Williamson, J. D. Schuddebeurs, P. J. Norman, C. D. Booth, G. M. Burt and J. R. McDonald, “Propulsion drive models for full electric marine propulsion systems,” IEEE Transactions on Industry Applications, vol. 45, no. 2, pp. 676-684, Mar. 2009.

[2] G. Sulligoi, A. Vicenzutti and R. Menis, “All-electric ship design: from electrical propulsion to integrated electrical and electronic power systems,” IEEE Transactions on Transportation Electrification, vol. 2, no. 4, pp. 507-521, Dec. 2016.

[3] W. A. Hill, G. Creelman and L. Mischke, “Control strategy for an icebreaker propulsion system,” IEEE Transactions on Industry Applications, vol. 28, no. 4, pp. 887-892, Jul. 1992.

[4] C. Hodge, B. Yin, X. Pei, F. Eastham, X. Zeng, O. Simmonds, “The implementation of a dual wound machine using a fractional slot winding,” in International Naval Engineering Conference and Exhibition, Oct. 2020.

[5] B. Yin, X. Pei, X. Zeng, F. Eastham, C. Hodge, and O. Simmonds, “Design and analysis of dual wound machine for electric ships,” in International Conference on Electrical Machines, Gothenburg, Aug. 2020.

[6] R. Sousaferreira and A. C. Ferreira, "Analysis of end-windings influence on the transient voltage distribution in machine stator windings by a three-phase model," in IEEE Transactions on Energy Conversion, vol. 36, no. 3, pp. 2110-2119, Sep. 2021.

[7] W. Wang, L. Wu and J. Zhu, "Influence of end-winding on optimal design parameters for maximum torque of DC excited flux-switching machines," 2019 22nd International Conference on Electrical Machines and Systems (ICEMS), Harbin, China, 2019, pp. 1-6.

[8] S. Williamson, M. R. E. Ellis, “Influence of rotor currents on end-winding forces in cage motor,” IEE Proceedings. Vol. 135, Pt B, No. 6, pp 371–379, Nov. 1988.